Journal Pre-proof

Quantifying the Level of Erosion-Induced Hazard on Riverbank

Wisam R. Muttashar, Usama Q. Al-Whaely, Dawod S.B. Almayahi, Meelad A. Hussein, Qassim M. Al-Aesawi, Ali A. Lafta, Michael E. Kalinski, Ali K.M. Al-Nasrawi, Brian G. Jones, Sajjad K. Chassib

PII: S2666-5921(25)00020-4

DOI: https://doi.org/10.1016/j.nhres.2025.02.007

Reference: NHRES 245

To appear in: *Natural Hazard Research*

Received Date: 6 September 2024

Revised Date: 22 February 2025

Accepted Date: 22 February 2025

Please cite this article as: Muttashar, W.R., Al-Whaely, U.Q., Almayahi, D.S.B., Hussein, M.A., Al-Aesawi, Q.M., Lafta, A.A., Kalinski, M.E., Al-Nasrawi, A.K.M., Jones, B.G., Chassib, S.K., Quantifying the Level of Erosion-Induced Hazard on Riverbank, *Natural Hazard Research*, https://doi.org/10.1016/j.nhres.2025.02.007.

Quantifying the Level of Erosion-Induced Hazard on Riverbank

Wisam R. Muttashar[a*], Usama Q. Al-Whaely[b], Dawod S.B. Almayahi[a], Meelad A. Hussein[b], Qassim M. Al-Aesawi[a], Ali A. Lafta[a], Michael E. Kalinski[c], Ali K. M. Al-Nasrawi[d], Brian G. Jones[e], and Sajjad K. Chassib[a]

[a] **Marine Science Centre, the University of Basrah, Basrah, 61004, Iraq.**

[b] **College of Marine Science, University of Basrah, Basrah, 61004, Iraq.**

[c] **Department of Civil Engineering, University of Kentucky, KY, 40506, USA.**

[d] **Department of Geography, University of Babylon, Hillah, Babylon, 51001, Iraq.**

[e] **School of Earth, Atmospheric and Life Sciences, University of Wollongong, Wollongong, NSW 2522, Australia**

[*] **Corresponding Author: wisam.muttashar@uobasrah.edu.iq**

Abstract

One of the most damaging and costly geoengineering hazards is riverbank erosion. This study aims to comprehensively determining and mapping hazard Levels of the riverbank subjected to erosion, along the tidal Shatt al Arab River, as a case study, southern Iraq. This research employs hydrological, sedimentological and geotechnical measurements to analysis the susceptibility level of the riverbank's stability. The ratio between the ebb and flood shear stress and the soil bank materials' critical shear stress was suggested as a practical way to comprehensively determine instability levels against erosion. Accordingly, the results showed that the southern and central stretches of the river have hazardous (< 1.0) or critical (between 1.0–2.0) states of the shear stress ratio, while the northern stretch is in a stable state, typically ranging between 2.0–3.0 but may exceed 4.0.

The northern river stretch, where soil layers have less susceptibility to erosion, corresponded to no change in the meanders (no-lateral migration indicated from the satellite imagery data) over the 48-year interval 1972-2020. The northern part of the river has stable conditions on the riverbanks and are gaining soil at a slight deposition rate of about 0.5 m/yr. In comparison, the southern river part showed that the meanders most likely agreed with the satellite imagery data which were prone to erosional processes and loss of bank materials.

It suggests that the shear stress ratio is a key to practically identify erosion-induced bank levels of tidal rivers and it could be used to develop strategies for mitigating the problem. The assessment of riverbank instability levels using the ratio of critical soil shear stress to fluid shear stress is a comprehensive, plausible way to better understand the susceptibility of tidal rivers.

Keywords: riverbanks, erosion, tidal rivers, Shatt Al-Arab.

1 Introduction

Despite the steady landscape features, tidal rivers (salt marsh streams) are known to be very sinuous planforms with highly undercut banks and significant bank erosion rates (Gabet, 1998). The erosional streambank process is a continuous critical process in which this hydrodynamic (fluvial) action surpasses the resistive strength of riverbank particles (Sutarto et al., 2014), resulting from inter-particle bonding (Ravisangar et al., 2005). It is the mechanism to be focused on when assessing streambank instability and rates of streambank erosion which have been interested field for the researches (Zhao et al., 2022; Hasanuzzaman, et al., 2023; Saikia and Mahanta, 2024) attempting to quantifying retreat impacts of the riverbanks due to erosion processes.

The distribution and magnitude of erosion rate and meander migration are highly variable because they are influenced by a variety of factors, including catchment area, bank material, local slope, configuration of water currents, water level, and position on a specific bend in a meander (Hooke, 1980; Abam, 2003), which become more complex when the riverbank sediment is cohesive (Das et al., 2019). Water current velocity is critical in characterizing the flow channel and assessing the erosion rate (Kang and Chan, 2022). In an inland river, where no tidal effects, flow only occurs in one direction and the water velocity is relatively constant; thus, it follows only one direction and magnitude of forces acting on the soil particles in the bed and bank. With tidal rivers, two water velocities correspond to the tidal ebb and flood currents that produce fluid shear stress that act in different directions and magnitudes on the particles. The Shatt al Arab River, being part of a semi-diurnal tidal system, exhibits two distinct hydraulic behaviors corresponding to flood and ebb currents daily (Al-Asadi et al., 2023; Lafta 2021). It experiences two 6-hour periods of either flooding or ebbing, with each period having opposite hydraulic characteristics in terms of water speed direction and magnitude. This is characteristic of the tidal Shatt al Arab River (TSAR) (Lafta 2021; Albadran et al., 2002).

The TSAR has been identified as a natural tidal meandering stream that has historically undergone instability and erosion of its banks (Albahili, et al., 2009; Albadran, et al., 2002). These dynamic banks and lateral changes, as shown in Figure 1, cause remarkable changes in the water boundary between Iraq and Iran, which has required frequent morphological surveys to monitor the shifting of the water boundary between the two countries (Albahili, et al., 2009). Studies have indicated that the limited understanding of tidal streambank instability in places such as TSAR comes from the complexity of a large number of relevant parameters that control the slope failure mechanism, including the hydrological river conditions, soil types, and plant distribution (Abam, 1993). Few studies (Albahili, et al., 2009; Albadran, et al., 2002) addressing this effect on the instability of the TSAR banks have been performed. In the case of the TSAR, studies have only addressed specific locations along the river.

This paper provides a profound analysis of streambank stability parameters of tidal rivers by taking the TSAR as a case study. It focuses on how two hydrologic conditions, namely, the tidal ebb and flood shear stresses, affect the riverbanks by setting a ratio between the two tidal (ebb and flood) shear stresses and the bank materials' critical (soil) shear stress. This ratio can be applied to determine riverbank stability levels against erosion and lateral migration. The paper employed three field measurements and analyses, including hydrological, geotechnical, and satellite images, to evaluate the riverbanks erosion and retreat level of the tidal meandering river.

The significance of this research is to provide a comprehensive and practical approach to understanding the susceptibility of tidal riverbank instability. It simplifies the complexities associated with bank stability in tidal rivers.

2 Theoretical background

The failure of streambanks occurs through processes causing either a decrease in shear strength or an increase in shear stresses of the soil mass (*M*) (Abramson et al., 2001). Both types of these processes act on the riverbanks. According to previous studies and preliminary observations, slope failure of the TSAR banks results from the fluvial processes, on which the solutions should be focused (Das 2019; Sutarto et al 2014). The fluvial process can be presented using the average applied fluid shear stress, τ_a, as a parameter showing the hydraulic river characteristics:

$$\tau_a = \gamma_w dS \quad , \qquad (1)$$

where γ_w is the unit weight of water (kN/m^3), *d* = water height above midpoint (*m*), and *S*=slope of the energy grade line, approximated by the channel slope. This fluid shear stress (τ_a) is a crucial indicator of the erosion process on the bank by comparing the fluid shear stress with the critical shear stress of the riverbank material (τ_c). The critical shear stress expresses the strength of the soil consisting of the riverbanks and beds. Soil erosion takes place if τ_a exceeds τ_c.

Both τ_a and τ_c are well correlated to the rate of erosion of the riverbanks, and the erosion rate (ε) can be estimated as a function of τ_c. When τ_a exceeds τ_c, the lateral erosion distance is then considered and estimated (Osman and Thorne, 1988). Thus, lateral erosion can be implied as to the Factor of Safety (*FS*):

$$\varepsilon = FS = \frac{\tau_c}{\tau_a}. \qquad (2)$$

Soil properties seem the crucial factor in evaluating the bank stability against the hydraulic factors of the river. Léonard and Richard (2004) developed a significant relationship between τ_c and undrained shear strength (S_u), as described in Equation 3. The relationship (Equation 3) was statistically significant (P-value<0.01) with a high coefficient of correlation (R^2=0.93). The standard error for the estimated slope value of the regression, noted as β in Equation 3, is about 1.2x10^{-5}.

$$\tau_c = \beta(S_u)\,, \qquad (3)$$

The β (2.6 x 10^{-6}) is a dimensionless constant equal to, resulted from experimental tests. In this study, undrained shear strength measured through the geotechnical tests of the selected banks was used to estimate the critical shear stress (τ_c).

Regarding the fluid shear stress (τ_a), and because of the tidal river conditions, the speed and directions of the ebb and flood currents are the most significant hydrological parameters of the riverbed and bank erosional processes. These tidal ebb and flood currents do not appear to be evenly distributed in the tidal rivers (Lafta 2021). Two behaviors of the velocities that produce two or more shear stresses, τ_a, acting differently in direction and magnitude on the particles.

The hydraulic shear stress, τ_a, is a vital function of water current velocity (u) and its change affects the magnitude and directions of the shear forces acting on the bed or bank particles. The TSAR case is described as a semi-diurnal tidal river, meaning that TSAR has two hydraulic behaviors (flood and ebb tides) daily at approximately 6 hours for each behavior (Lafta 2021). As a result, TSAR's flood and ebb currents act at two hydraulic statuses in terms of velocity direction and magnitude, acting uniformly. The first hydraulic status is the norm flow (current), in which the river inflow and the ebb currents run in the same direction. The speed of the currents is doubled and higher than that of the second (flood) tide status. Conversely, in the flood river status, the direction of the flood currents is opposite to the river inflow, causing the currents' direction to change and reduce water speed (u). In this event, the (opposite) currents (at the flood period) can be referred to as a negative sign ($-u$), while the water currents, running at norm conditions toward the downstream (at the ebb time), can be noted as a positive sign ($+u$). Consequently, two shear stresses ($+\tau_a$ and $-\tau_a$) will act differently on the bed and bank particles. Hence, two cases of the tidal river should be considered when the effect of the fluid shear stress on the grains to detach is analyzed. Figure 2 shows a simplification sketch to illustrate the concept of the two actions of the shear stresses ($+\tau_a$ and $-\tau_a$) at the two tide conditions on the grain. Therefore, this research examines the two-fluid shear stresses determined at the tidal flood and ebb currents, noted as τ_{a_Flood} and τ_{a_Ebb}, respectively, whether they are greater or less than critical shear stress, τ_c.

Thus, Equation 1 could be expressed as $\tau_{aEbb} = +\gamma_w dS$ at tidal ebb conditions, and $\tau_{aFlood} = -\gamma_w dS$ at tidal flood conditions.

Alternatively, if two-point velocities in a vertical profile at two depths (y_1 and y_2) are known (rather in the lower 15 percent of the depth), the local shear stress on the bed can be determined from the following (Richardson et al., 2001):

$$\tau_a = (\rho_w v^2)/[(5.75 * \left(Log\left(\frac{12.27 * y_1}{Ks}\right)\right)]^2 \text{ . } (4)$$

where, y_1 is the flow depth, K_s is height roughness which can be obtained from the grain roughness n (Chow 1959), and v is the average velocity in the vertical.

Equation 4 is valid for fully turbulent uniform flow over a hydraulically rough boundary in wide channels with a plane bed (Richardson et al., 2001). Therefore, Equation 4 can be applied twice, when v is the velocity of the river currents at ebb time, and when v is the velocity of the river currents at flood time.

After determining τ_c and checking if $\tau_a \geq \tau_c$, bank erosion exists. To test the required parameters to evaluate the erosion and instability levels of the TSAR's riverbanks, field hydrological and geotechnical measurements and satellite images were performed to evaluate the long-term lateral migration of the river.

3 Methods and Materials

3.1 Site Description

The TSAR originates at the Qurna site at the confluence of the Tigris and Euphrates Rivers about 65 km north of Basrah. The TSAR flows around 115 km to the south within Iraq, forms the border with Iran downstream for another 85 km and empties into the Persian Gulf as shown in Figure 3 (Alkhafaji et al., 2023). The TSAR flows about 200 km overall with a width ranging between 330 m at the confluence of the Tigress and Euphrates Rivers to 1,250 m at the Persian Gulf, and depths ranging from 8.5-24 m at the confluence and Persian Gulf, respectively (Al-Asadi and Muttashar, 2022). The TSAR experiences predominantly semi-diurnal tide regimes.

With different size-scale curvatures, geomorphologically, TSAR has around 15 meanders, estimated from the satellite images and shown in Figure 3 noted as M-01 through M-15. The current study focused on these curvatures to implement the measurements.

Regarding the sediment, the study area is part of the lower Mesopotamian sedimentary plain of southern Iraq which experiences complex fluvial-estuarine processes of the Shatt al Arab delta, and the fine-grained sediments are the most dominant deposits (Alfaris et al., 2024; Muttashar et al., 2021). Figure 4 shows grain size distribution curves of five sites that reveals generally clayey silt to silty clay sediment in the TSAR.

The hydrological characteristics of TSAR depend mainly on its four tributaries, which include the Tigris and Euphrates Rivers. The tidal regime of TSAR is a mixed type between diurnal and semi-diurnal, where the latter is the more predominant. The tide ranges from about 0.5 m at the Qurna location to 3 m at the Faw location (Al-Ramadhan and Pastour, 1987). In the study presented herein, the investigated sites were chosen to sample, test, and analyze the bank slides and slope stability at the maximum curvatures of TSAR and locations with high velocities relatively near the river banks. The weakest slide-prone sites are mostly identified in the positions of maximum curvature of the river since the toe of the slope is subjected to a relatively high-water velocity, which in turn causes disturbance and scouring of the slope toe and rendering the failure (Abramson et al., 2001). Figure 3 shows the location map of the study area, including the site locations.

3.2 Data collection and field measurements

The data can be summarized into three categories; Field hydrological, geotechnical, and satellite data (images) that were used to evaluate the long-term lateral change of the TSAR riverbanks.

For the geotechnical testing, the main purpose of the geotechnical data is to detect the critical shear stress (τ_c) dependent on the mechanical parameter of the soil layers of the river banks, such as shear strength and unconfined compression strength, along a selected riverbank side of the TSAR. To do so, geotechnical data were collected to define the main shallow riverbank layers (4-

5 m). Several soil data sources (Saeedy and Mollah 1990; Muttashar et al., 2012; Muttashar et al., 2024) are integrated with the field measurements to cover the investigated area. Figure 2 shows ten selected sites (boreholes) to implement field soil testing evenly distributed along the river at its banks. Each borehole was dug to a depth of 4-5 m. Geotechnical testing included Grain size distribution analysis, Atterberg limits, water content tests, unconfined compressive strength testing and undrained triaxial shear strength testing according to applicable American Society for Testing and Materials (ASTM) standards.

For the hydrological measurements, data were acquired using an Acoustic Doppler Current (Velocity) Profiler (ADCP) and measuring water velocities at several vertical profiles in the outer-bank region, as shown in Figure 5. These field measurements were performed by the Marine Science Center at the University of Basrah. The measured parameters included depth (d), water velocity (v) throughout the water column and cross-section area and Manning number (roughness; n), in addition to the slope (S) of the TSAR. These hydrological parameters are essential to estimate the fluid shear stress (τ_a) at the selected sites and subsequently estimate the short-term erosion rate of the river banks. The field measurements include 13 hours at each site to characterize the hydrological behavior of the river during the two flood and ebb tide periods.

For the long-term change in riverbanks, satellite images taken in June 1972, June 1986, June 2000 and June 2020 from the Landsat satellite 1, 5, 7, and 8 were employed and analyzed to determine lateral migration rates. In this study, these remotely sensed data over the 48 years are accessible and have sufficient resolution, and have been used in other prior studies (Lawler, 1993; Jin et al., 2022; Lo et al., 2021) for determining lateral migration of the river banks at meandering sites as well as unstable slopes and their movement characteristics (Dwivedi et al., 2023; Wang et al., 2024). Table 1 lists the details of the satellite images used for this study. It is notable to mention that the column " Flood Tide Conditions" shows the water level of tide at the time where these satellite images have been taken.

Table 1 Details of the satellite images from 1972, 1986, 2000 and 2020 used to assess to the lateral migration changes as part of this study.

Spacecraft Id	Sensor Id	Path	Row	Date Acquired	Scene Center Time	Flood Tide Conditions
LANDSAT_8	OLI	165	39	2020-06-22	07:15:35 AM	2.0m
LANDSAT_8	OLI	166	39	2020-06-13	07:21:41 AM	2.4 m
LANDSAT_5	TM	165	39	2000-06-15	06:52:13 AM	2.0 m
LANDSAT_7	ETM+	166	39	2000-08-01	7:13:13 AM	1.7 m
LANDSAT_5	TM	165	39	1986-06-09	06:39:49 AM	1.7 m
LANDSAT_5	TM	165	39	1986-06-16	06:45:46 AM	2.7 m
LANDSAT_1	MSS	177	39	1972-09-05	06:45:21 AM	2.4 m
LANDSAT_1	MSS	178	39	1972-08-01	06:50:52 AM	1.9 m

4 Results

4.1 Remotely sensed changes

Figures 6 and 7 show the changes of six typical meanders (M-01, M-04, M-05, M-07, M-08 and M-09) at the river over the entire 48-year time frame from 1972-2020. Figure 6 is a descriptive delineation of the river shorelines at these four periods, which turned out little changes in lateral migration history, where the long-term lateral migration of the bank soils responds differently and sometimes exhibited non-uniform responses that were quantified in Figure 7. The maximum loss (retreat) and gaining soil of the banks are about (-40) and (+30) m, respectively, as a lateral movement of the banks at the selected sites. The maximum estimated long-term rate is between (+0.6) to (-0.8) m/yr. The meanders have generally not revealed significant retreat or building (gaining new soil) through those four periods.

4.2 Geotechnical consideration of the selected sites

Figure 8 shows the general geotechnical section of the soil layers along the TSAR banks from Qurna (upstream) to Faw (downstream). The modified diagram (Figure 8) is built from a number of boreholes that were excavated longitudinally from Qurna to Faw along the TSAR banks. The section shows shallow soil layers not exceeding 5 m in thickness that are most prone to instability conditions. The soils reflecting the river bank deposits mainly consist of soft clays and silts, varying slightly at different locations between Qurna to Faw.

The riverbank consists almost entirely of fine-grained sediments, and the face of the cut bank shows mainly two horizontal layers formed by stiff, medium stiff, soft, or very soft silty clayey and clayey silt with few sand particles. The consistency characteristics of these layers reflect low to intermediate levels of plasticity with non-active soil behavior because of the low content of active smectite mineral groups in their composition (Muttashar et al., 2021; Muttashar et al., 2020).

Table 2 summarizes the geotechnical characteristics of the soil layers of the riverbanks prone to fluvial actions and instability at each site taken in this study at the Faw, Seeba, Ashar and Sweep locations. Each borehole was characterized into two soil layers as described in Table 2. The shear strength parameter of these layers is mainly 74-37 kPa and 17-18 kPa of the first and second layers, respectively. Shear strength (*Su*) is a crucial state soil parameter to determine the resistance of the bank material against erosion since the critical shear stress, τ_c, is practically a function of S_u. Also, Table 2 also includes the estimated τ_c of each detected soil layer.

Table 2 Geotechnical Properties required to calculate critical shear stress.

Boreholes (BH)	Near-surface soil Layers	Depth (m)	Description	Shear Strength, S_u (kPa)	Critical (soil) shear stress, τ_c (Pa)
BH-01	Layer-1	0-2	M.stiff to stiff sandy silty clay	37	10
	Layer-2	> 2	Soft brown silty clay	18	5
BH-02	Layer-1	0-2	V.Stiff Clayey silt	60	15
	Layer-2	2_4.5	M. Stiff to soft Clayey silt	20	5
BH-03	Layer-1	0-3	Stiff Silty clay	50	13
	Layer-2	3_5	M. Stiff Silty clay	30	8
BH-04	Layer-1	0-3	Stiff Silty clay	34	9
	Layer-2	3_5	M. Stiff Silty clay	17	4
BH-05	Layer-1	0-1.5	M.stiff clay and silty clay	53	14
	Layer-2	1.5->4	Soft gray elastic silt	14	4
BH-06	Layer-1	0-2	Stiff to M.stiff Silty clay	23	6
	Layer-2	2_5	v. soft to soft Clayey Silt	7	2
BH-07	Layer-1	0-1.5	Stiff silty clay	59	15
	Layer-2	1.5-4	soft clayey silt with sand	17	4
BH-08	Layer-1	0-2	Stiff Clayey Silt	140	36
	Layer-2	2_5	V.soft to soft Clayey Silt	9	2
BH-09	Layer-1	0-2	Stiff Silty clay	34	9
	Layer-2	2_4	Soft silty clay	10	3
BH-10	Layer-1	0-2	M. Stiff Silty clay	23	6
	Layer-2	2_5	V soft to soft clayey Silt	7	2

4.3 hydrological properties and water velocity behavior.

Figure 9 shows the directions of the ebb and flood tidal currents coinciding with the velocity distribution at three locations: Qurna, Seeba, and Faw. The ebb current azimuth direction is between 75^0 and 125^0 while the flood tidal current direction is greater than 250^0. As the current moves from the ebb to the flood phase, or vice versa, the current switches direction and increases in velocity.

From the figure, the ebb currents are generally shorter in duration but a higher velocity than the flood currents. So, in both tides (flood and ebb), the currents in any specific site have almost the same values. For the Faw site, water speed ranges between 0.64 m/s at the ebb tide to 0.52 m/s at the flood tide. For Seeba, speeds values are between 0.70 m/s at the ebb tide to 0.50 – 0.55 m/s at flood tide. At the Sweep site, the water speed ranges from 0.35-0.40 m/s at ebb tide to 0.25 m/s at flood tide. The ebb current is taking place at less time, but a higher amount than the time of flood currents, is a day which generally reveals asymmetric tidal current behavior. In both phases (flood and ebb), the currents in any specific site have almost the same values. However, Figure 10 shows the behavior of the velocity change over normalized depths (z/h) at the three sites, where depth z is normalized relative to total river depth h. It shows the effects of the ebb and flood phases through velocity profiles over time, affecting the shear velocity's uniform behavior with depth. At the downstream sites, Faw site, and even the Seeba site, the uniform replacement between the water masses is evident during the ebb and tidal flood phases. The high and low velocities vertically replace space, corresponding to the tidal phase change. However, it seems not adequately uniform and clear for these alternatives in tidal phases (ebb and flood) as it moves away from the sea toward the upstream Qurna site as shown in Figures 10e and 910f. It is necessary to understand the spatial and temporal descriptive behavior of the ebb and flood current velocities since it is relevant to determining the behavior of fluid shear stress τ_a.

Table 3 Hydrological Properties required to calculate fluid (applied) shear stress (τ_a).

Locations	Traverse No.	Height, *d* (m)	Measured velocity, *V* (m/s)	Manning coef.,, *n*	Shear velocity at flood time (-)U_{Flood}	Shear velocity at ebb time (+)U_{Ebb}	*Fluid shear stress, τ_a (Pa)	**Fluid shear stress at flood time, τ_{aFlood} (Pa)	**Fluid shear stress at ebb time, τ_{aEbb} (Pa)	$\tau_{aNet} = \tau_{aEbb} - \tau_{aFlood}$
Qurna	L-1	4	0.275	0.0239	0.08	0.35	1.24	0.242	5.270	5.028
Al-sharash	L-2	10	0.155	0.0239	0.24	0.31	3.09	1.868	3.118	1.250
Ektiban	L-3	13	0.183	0.0216	0.16	0.18	4.02	0.656	0.831	0.174
Al-Ashar	L-4	20	0.228	0.0188	0.26	0.3	6.19	1.235	1.7106	0.474
Abo flus	L-5	14	0.3	0.0319	0.28	0.3	4.33	3.978	4.568	0.589
Seehan	L-6	8	0.587	0.0262	0.51	0.54	2.48	10.684	11.977	1.294
Faw	L-7	10	0.645	0.0218	0.51	0.52	3.09	7.244	7.531	0.287

where *τ_a is the average applied (fluid) shear stress at the section midpoint calculated using (γ_w.d.S), while ** τ_a is the fluid shear stress predicted by Equation 4 (Richardson et al. 2001).

5 Discussion

Table 4 shows the ratio of (τ_c/τ_a) reflected as the predominated factor controlling the stability of selected outer riverbanks of TSAR (the 15 meanders).

Table 4 the ratio of τ_c/τ_a controlling the bank stability levels of selected outer riverbanks of TSAR (15 meanders).

BH	Near-surface soil Layers	Depth (m)	Critical (soil) shear stress, τ_c (Pa)	**Fluid shear stress at flood time, τ_{aFlood} (Pa)	**Fluid shear stress at ebb time, τ_{aEbb} (Pa)	τ_{aNet} (Pa)	$\tau_{c(ave.)}/\tau_{aFlood}$	$\tau_{c(ave.)}/\tau_{aEbb}$
BH-01	Layer-1: stiff	0-2	10	0.15	3.3	3.2	39.7	1.8
	Layer-2: Soft	> 2	5	0.15	3.3	3.2	18.6	1.0
BH-02	Layer-1: Stiff to very stiff	0-2	15	1.24	2.1	0.8	8.0	4.8
	Layer-2: Medium Stiff	>2	5	1.24	2.1	0.8	2.8	1.7
BH-03	Layer-1: Stiff	0-3	13	0.51	0.6	0.1	19.8	15.7
	Layer-2: Medium Stiff	>3	8	0.51	0.6	0.1	11.9	9.4
BH-04	Layer-1: Stiff	0-3	9	1.14	1.6	0.4	7.2	5.2
	Layer-2: Medium Stiff	>3	4	1.14	1.6	0.4	3.6	2.6
BH-05	Layer-1: Medium stiff	0-1.5	14	1.14	1.6	0.4	11.0	8.0
	Layer-2: Soft	>1.5	4	1.14	1.6	0.4	2.9	2.1
BH-06	Layer-1: Stiff to M.stiff	0-2	6	1.67	1.9	0.2	1.5	1.3
	Layer-2: v. soft to soft	> 2	2	1.67	1.9	0.2	0.5	0.4
BH-07	Layer-1: Stiff	0-1.5	15	6.04	6.8	0.7	1.4	1.3
	Layer-2: soft	> 1.5	4	6.04	6.8	0.7	0.4	0.4
BH-08	Layer-1: Stiff	0-2	36	5.48	5.7	0.2	5.0	4.8
	Layer-2: V.soft to soft	>2	2	5.48	5.7	0.2	0.3	0.3
BH-09	Layer-1:Stiff	0-2	9	1.14	1.6	0.4	7.1	5.2
	Layer-2: Soft	>2	3	1.14	1.6	0.4	2.1	1.5
BH-10	Layer-1: Medium Stiff	0-2	6	1.14	1.6	0.4	4.8	3.5
	Layer-2: very soft to soft	>2	2	1.14	1.6	0.4	1.5	1.1

where *τ_a is the average applied (fluid) shear stress at the section midpoint calculated using (γ_w.d.S), while ** τ_a is the fluid shear stress predicted by Equation 4 (Richardson et al. 2001).

In general, Figure 11 represents the values of τ_c/τ_a for the first stiff surface soil layer, while Figure 11 presents the τ_c/τ_a values for the second (soft) layer that ranges between 1.5-2.0 m in depth. In both Figures (11 and 12), the τ_c/τ_a values illustrate the two tides cases of the river, flood and ebb tides, in which the fluid shear stress τ_a is changed based on velocities of the river water at those two tide conditions as aforementioned. The two figures show the levels of change in τ_c/τ_a in the tonal form for both flood and ebb cases.

In Figure 11, τ_c/τ_a for the flood period is between 2.5 to 4.5, which is an acceptable value meeting the range of the stability of the river banks against the erosional processes and lateral migration. While at the ebb time, the τ_c/τ_a ranges between 2.0 to 4.5 meters. The difference between the two tidal states (Fig. 11a and 11b) is minimal, even though there is a change in the velocity of the shear stresses of the water currents in both cases. The shear strength of the surface soil layer (the stiff layer) is considered the essential control parameter that exceeds the water shear stresses in both tides.

However, the situation differs in the case of the second soft layer (at depths of 1.5-2.0). Figure 12 shows that these river bank values are subjected to erosion, and the banks are unstable. The value of τ_c/τ_a is less than 1.0 in the river meanders of the southern part (M-15, M-14, M13, M-12, M-11, M-10, M-09, M-08, M-07, and M-06), yet it is a less risky level relating to the northern part of the river (M-1, M-2, and M-4).It is noticed here that most changes in the soil shear strength properties of the second layer are in the northern part of the river at points (M-1, M-2, M-3, M-4), and it decreases towards the southern part of the river. All meanders of the south of to central river parts are within the hazardous values (< 1.0) or even critical (between 1.0-2.0). While the values in the northern part of the river range between 2.0-3.0 or more than 4.0.

The northern river part that soil layers with less susceptibility to erosion corresponded to no change in the meanders and no-lateral migration indicated from the satellite image data over the past 48 years between 1972-2020 as shown in Figure 5. Figure 5 reveals the meanders of the northern part of the river M-1, M-2, M-3 and M-4 stability conditions on the riverbanks with a deposition rate (gaining) of about 0.5 meters per year. The southern river part also seems to agree with what was obtained from the satellite image data (Figure 5). It shows that the meanders M-9, M-8, and M-7, as typical meanders of the southern part, are prone to erosional processes and loss of the bank soils. In this river part, since the tidal flow in the case of the TSAR banks acts in two inverse directions (flood and ebb shear stresses), this might cancel out the effectiveness of each shear stress to a certain degree. Furthermore, the flow action on the banks reduces to a minimum during the slack-water periods (no flow action) between the flood and ebb flows. As a result, the time that the failed block remains at the toe of the bank will be longer, which will help the failed materials to be maintained on the original bank before entraining. It can be concluded that the prolonged presence of failed materials near the bank toe, the occurrence of inverse ebb and flood tide movements, and the uniform soil composition throughout bank layers can be key factors that support more protection to the river bank itself against erosion processes in the case of tidal rivers.

5.1 Limitations and future research

This research has yet to further seek the duration of flow impact on the slump block at the toe of the bank. Additional investigation is required to examine the temporal influence of flood-dominated and ebb-dominated river flow on the failed block, and to juxtapose it with the temporal ramifications of non-tidal river flow. The presence of cyclic hydraulic action processes on the TSAR's bank is evident, and it plays a crucial role in the bank's stability, resulting in a minimal erosion rate of the bank soil.

6 Conclusions

This research is a comprehensive practical approach to evaluate the susceptibility of tidal riverbank instability, and simplifies the complexities associated with bank stability in tidal rivers. By taking

Tidal Shatt al-Arab River (TSAR) as a case study, this paper analyzes streambank instability levels and number of points can be concluded;

- Three tests and analyses, including hydrological, geotechnical, and satellite images, were used for the evaluation of the TSAR riverbanks.
- Based on its instability levels and hydrological river behavior, TSAR can be divided into two portions. All meanders south of the central river parts are within the hazardous (< 1.0) or even critical values (between 1.0-2.0) and are more prone to erosion. While the values in the northern part of the river range between 2.0–3.0 or more than 4.0.
- For the northern river part, the soil layers are less susceptible to erosion, corresponding to the no change in the meanders and no-lateral migration as indicated in the satellite image. Most meanders of the northern portion have a slightly positive (gaining) deposition rate of about 0.5 m/yr.
- In contrast, the southern river part showed that the meanders agreed with the satellite image data at specific sites prone to erosional processes and loss of bank soils.
- The developed ratio of critical (soil) shear stress of the river to the fluid shear stress of the river is a comprehensive plausible means of understanding better the susceptibility of the tidal riverbank instability. It can assist in understanding better the meander evolution based on the bank shear strength and the tidal ebb and flood current velocities.

Funding

The authors declare that no funding was received during the preparation of this research.

Declaration of competing interest

The authors declare that they have no known competing personal relationships or financial interests could have appeared to influence the work reported in this manuscript.

Acknowledgment

The authors acknowledge the university of Basrah, Iraq, for providing financial assistance and the Marine Science Center, Basra, Iraq, for providing the technical facilities during the research.

References

Abam, T.K.S., 1993. Factors affecting distribution of instability of river banks in the Niger delta. Engineering geology, 35(1-2), 123-133. https://doi.org/10.1016/0013-7952(93)90074-M.

Abramson, L.W., Lee, T.S., Sharma, S., Boyce, G.M., 2001. Slope stability and stabilization methods. John Wiley & Sons. ISBN: 978-0-471-38493-9.

Al-Asadi S.A., Muttashar, W.R., 2022. Impact of the Environmental Degradation of Rivers on the Reappraisal of International Agreements Related to the Transboundary Watercourse, Shatt Al-Arab River (Southern Iraq): A Case Study. Sustainable Water Resources Management, 8(3). https://doi.org/10.1007/s40899-022-00669-2.

Al-Asadi, S. A., Alhello, A. A., Ghalib, H. B., Muttashar, W. R., & Al-Eydawi, H. T. 2023. Seawater intrusion into Shatt Al-Arab River, Northwest Arabian/Persian Gulf. Journal of Applied Water Engineering and Research, 11(2), 289-302. https://doi.org/10.1080/23249676.2022.2113460.

Alfaris, M. A., Alrubaye, A. A., Muttashar, W. R., & Lo, E. 2024. The compression behavior of riverine fine-grained soils treated with organic matter. Soil and Environment. 43(2): https://doi:10.25252/SE/2024/243389.

AlKhafaji, H., Muttashar, W. R., & Al-Mosawi, W. M. 2023. Proposing an inflatable rubber dam on the Tidal Shatt Al-Arab River, Southern Iraq. Journal of the Mechanical Behavior of Materials, 32(1), 20220201. https://doi.org/10.1515/jmbm-2022-0201.

Al-Ramadhan, B., and Pastour, M., 1987. Tidal Characteristics of Shatt Al-Arab River Marina Mesopotamica 2:15-28.

Chow, V. T., 1959. "Open-Channel Hydraulics, McGrow-Hill Book Company." Inc. New York. P. 206.

Das, V.K., Roy, S., Barman, K., Debnath, K., Chaudhuri, S., Mazumder, B.S., 2019. Investigations on undercutting processes of cohesive river bank. Engineering Geology, 252, 110-124. https://doi.org/10.1016/j.enggeo.2019.03.004.

Dwivedi, D.K., Saraf, A.K., Das, J.D., 2023. Geoinformatics-based investigation of slope failure and landslide damming of Chenab River, Lahaul-Spiti, Himachal Pradesh, India. Natural Hazards Research, 3(2), 186-195. http://dx.doi.org/10.1016/j.nhres.2023.02.008.

Gabet, E. J., 1998. Lateral migration and bank erosion in a saltmarsh tidal channel in San Francisco Bay, California, J. Estuaries, 21(4), 745-753. https://doi.org/10.2307/1353278.

Hasanuzzaman, M., Islam, A., Bera, B., Shit, P.K., 2023. Quantifying the riverbank erosion and accretion rate using DSAS model study from the lower Ganga River, India. Natural Hazards Research. https://doi.org/10.1016/j.nhres.2023.12.015.

Hooke, J.M., 1980. Magnitude and distribution of rates of river bank erosion, Earth Surface Processes, 5(2), 143-157. https://doi.org/10.1002/esp.3760050205.

Jin, J., Chen, G., Meng, X., Zhang, Y., Shi, W., Li, Y., ... Jiang, W., 2022. Prediction of river damming susceptibility by landslides based on a logistic regression model and InSAR techniques: A case study of the Bailong River Basin, China. Engineering Geology, 299, 106562. https://doi.org/10.1016/j.enggeo.2022.106562.

Kang, C., Chan, D., 2022. Investigation of erosion characteristics of debris flow based on historical cases. Engineering Geology, 306, 106767. https://doi.org/10.1016/j.enggeo.2022.106767.

Lafta, A. A., 2021. Estimation of Tidal excursion length along the Shatt Al-Arab estuary, southern Iraq. Vietnam Journal of Science and Technology, *59*(1), 79-89. https://doi:10.15625/2525-2518/59/1/15433.

Lawler, D.M., 1993. The measurement of river bank erosion and lateral channel change: a review. Earth surface processes and landforms, 18(9), 777-821. https://doi.org/10.1002/esp.3290180905.

Léonard, J., Richard, G., 2004. Estimation of runoff critical shear stress for soil erosion from soil shear strength. Catena, 57(3), 233-249. https://doi.org/10.1016/j.catena.2003.11.007.

Lo, P.C., Lo, W., Chiu, Y.C., Wang, T.T. 2021. Movement characteristics of a creeping slope influenced by river erosion and aggradation: Study of Xinwulü River in southeastern Taiwan. Engineering Geology, 295, 106443. https://doi.org/10.1016/j.enggeo.2021.106443.

Muttashar, W. R., Bryson, L. S., McGlue, M., & Woolery, E. 2020. The integration of grain-size distribution and plasticity parameters for characterizing and classifying unconsolidated fine-grained sediments. Bulletin of Engineering Geology and the Environment, 79, 925-939. https://doi.org/10.1007/s10064-019-01588-x.

Muttashar, W.R., Al-Aesawi, Q.M., Al-Nasrawi, A.K., Almayahi, D.S., Jones, B.G., 2024. Coastline instability evaluation: multitemporal bathymetric mapping and sediment characteristics. Environmental Earth Sciences, 83(1), 43. https://doi.org/10.1007/s12665-023-11375-3.

Muttashar, W.R., Al-Mosawi, W.M., Al-Aesawi, Q.M., Abas, N.S. 2012. Detection of subsurface layers by Sub Bottom Profiling (SBP) of cross section of Shatt Al-Arab River at Al-Rebat branch, Basrah, southern Iraq. Mesopotamian Journal of Marine Sciences, 27(1), 49-58. http://dx.doi.org/10.58629/mjms.v27i1.171.

Muttashar, W.R., Bryson, L.S., Al-Humaidan, Z.A., 2021. The use of particle size distribution integrated with consistency limits for experimentally simulating fine-grained sedimentary units. Arabian Journal of Geosciences, 14(22), 1-12. https://doi.org/10.1007/s12517-021-08812-7.

Osman, A.M., Thorne, C.R., 1988. Riverbank stability analysis. I: Theory. Journal of Hydraulic Engineering, 114(2), 134-150. http://dx.doi.org/10.1061/(ASCE)0733-9429(1988)114:2(134).

Ravisangar, V., Sturm, T.W., Amirtharajah, A., 2005. Influence of sediment structure on erosional strength and density of kaolinite sediment beds. Journal of hydraulic engineering, 131(5), 356-365. https://doi.org/10.1061/(ASCE)0733-9429(2005)131:5(356).

Richardson, E.V., Simons, D.B., Lagasse, P.F., 2001. River engineering for highway encroachments: Highways in the river environment. Report No. FHWA-NHI-01-004, United States Federal Highway Administration.

Saeedy, H.S., Mollah, M.A., 1990. Geotechnical study of the North and Northwest Coast of the Arabian Gulf. Engineering Geology, 28(1-2), 27-40. https://doi.org/10.1016/0013-7952(90)90032-V.

Saikia, M., Mahanta, R., 2024. Riverbank Erosion and vulnerability–A study on the char dwellers of Assam, India. Natural Hazards Research, 4(2), 274-287. https://doi.org/10.1016/j.nhres.2023.10.007.

Sutarto, T., Papanicolaou, A.N., Wilson, C.G., Langendoen, E.J., 2014. Stability analysis of semicohesive streambanks with CONCEPTS: Coupling field and laboratory investigations to quantify the onset of fluvial erosion and mass failure. Journal of Hydraulic Engineering, 140(9), 04014041. http://dx.doi.org/10.1061/(ASCE)HY.1943-7900.0000899.

Wang, Y., Gao, H., Liu, S., Yang, D., Liu, A., Mei, G., 2024. Landslide detection based on deep learning and remote sensing imagery: A case study in Linzhi City. Natural Hazards Research. https://doi.org/10.1016/j.nhres.2024.07.001.

Figure 1 Dynamic and lateral changes of Shatt al Arab river banks.

Figure 2. Two actions of the shear stresses (τ_{a_Flood} or - τ_{a}) and (τ_{a_Ebb} or + τ_{a}) of the two tides conditions on the particle.

Figure 3. Location map of the TSAR and 15 meanders M-1 through M-15 identified in the satellite image.

Figure 4. Grain size distribution curves of five sites showing generally clayey silt to silty clay sediment.

Figure 5. Typical field ADCP measurement showing a Cross-section of the flow velocity distribution at the Qurna site.

Figure 6. Typical meanders M-01, M-04, M=-05, M-07, M-08 and M0-9 used to reveal the lateral migration history.

Figure 7. Loss (retreat) and building (gaining) bank soil estimated from the analysis of satellite images analyeis during the 1972-2020 time period.

Figure 8. Generalized geotechnical section of the layer, modified after (Albadran and Mahmood 2006).

Figure 9. Tidal current velocity behavior of TSAR (direction and speed) during a 13-hour period.

Figure 10. descriptive behavior of the ebb and flood tidal velocities at the three sites (Faw, Seeba, and Qurna).

Figure 11. Riverbank stability levels map of TSAR of the first stiff surface soil layer in two the tides conditions (ebb and flood). (Wisan, fix figure a so it says τ_c/τ_a instead of $\tau_{c}\_\tau_{a}$)

Figure 12. Riverbank stability levels map of TSAR of the second stiff surface soil layer in two the tides conditions (ebb and flood).


An old military checkpoint constructed
on the riverbank several decades ago

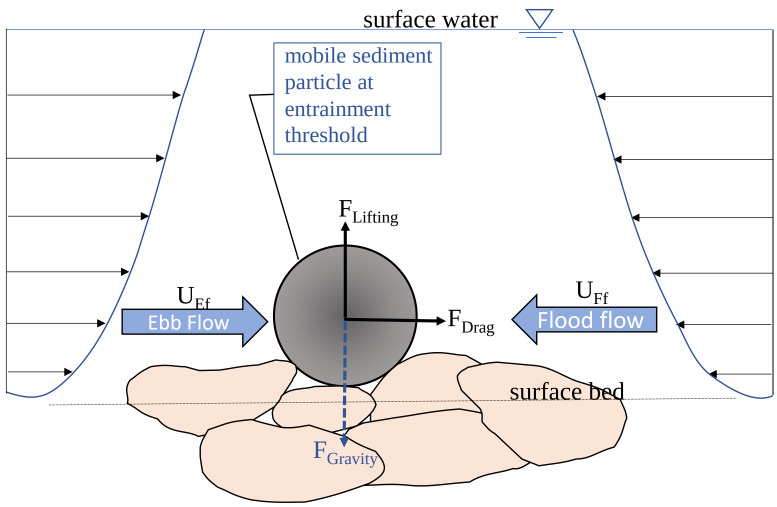
surface water
mobile sediment particle at entrainment threshold
F_Lifting
U_Ef
Ebb Flow
F_Drag
U_Ff
Flood flow
surface bed
F_Gravity

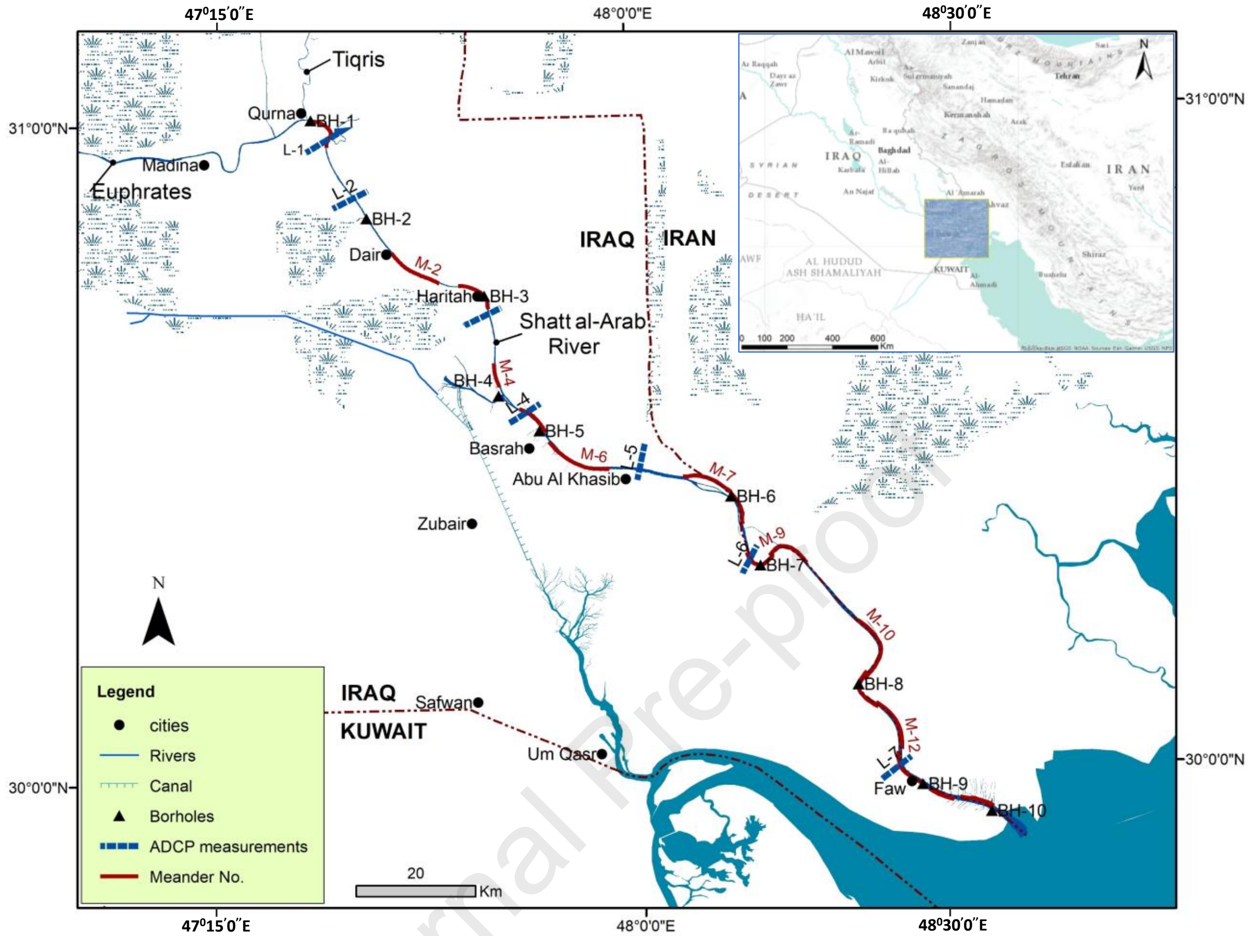

47°15′0″E
48°0'0"E
48°30′0″E
31°0'0"N
30°0'0"N
Tiqris
Qurna
BH-1
L-1
Madina
Euphrates
L-2
BH-2
Dair
M-2
Haritah
BH-3
Shatt al-Arab River
M-4
BH-4
L-4
BH-5
Basrah
M-6
L-5
Abu Al Khasib
M-7
BH-6
Zubair
M-9
L-6
BH-7
M-10
BH-8
M-12
L-7
BH-9
Faw
BH-10
IRAQ
IRAN
IRAQ
KUWAIT
Safwan
Um Qasr
Legend
cities
Rivers
Canal
Borholes
ADCP measurements
Meander No.
20
Km
N

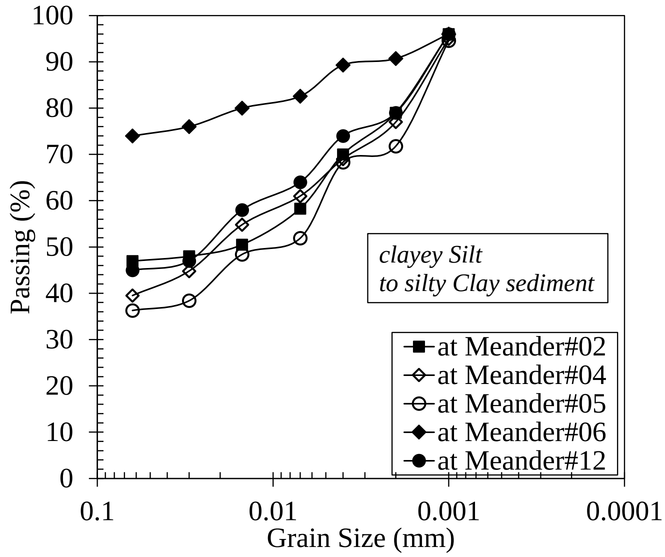
Passing (%)
100
90
80
70
60
50
40
30
20
10
0
0.1
0.01
0.001
0.0001
Grain Size (mm)
clayey Silt
to silty Clay sediment
at Meander#02
at Meander#04
at Meander#05
at Meander#06
at Meander#12

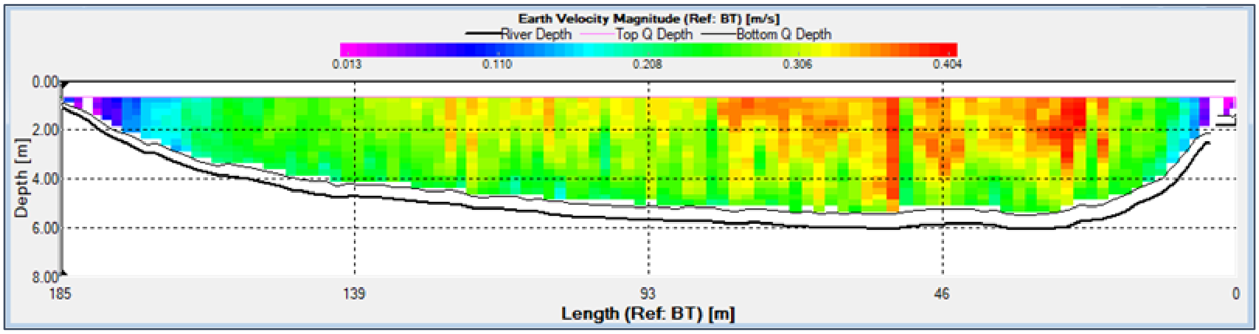
Earth Velocity Magnitude (Ref: BT) [m/s]
River Depth
Top Q Depth
Bottom Q Depth
0.013
0.110
0.208
0.306
0.404
0.00
2.00
4.00
6.00
8.00
Depth [m]
185
139
93
46
0
Length (Ref: BT) [m]

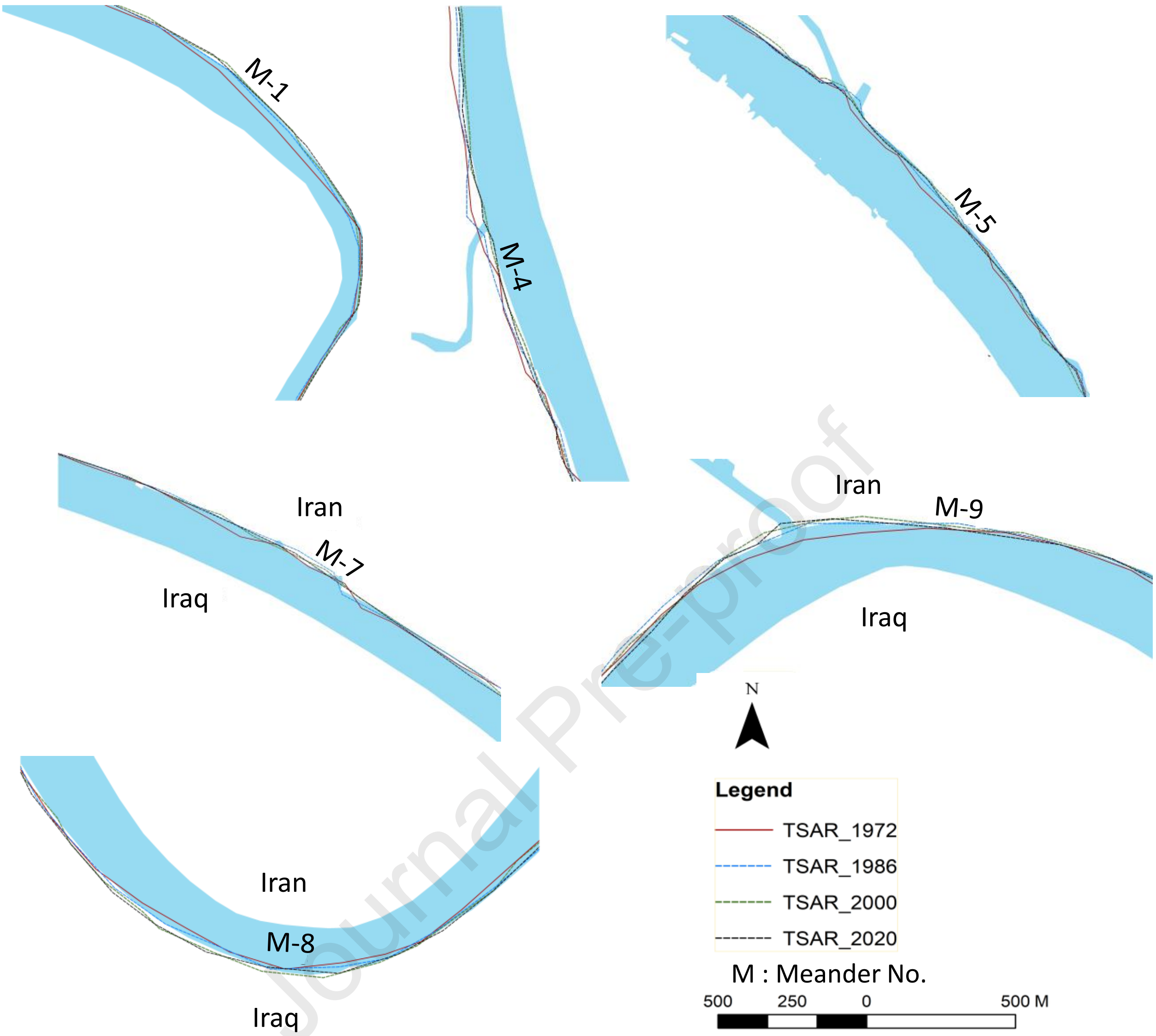
M-1
M-4
M-5
Iran
M-7
Iraq
Iran
M-9
Iraq
Iran
M-8
Iraq
N
Legend
TSAR_1972
TSAR_1986
TSAR_2000
TSAR_2020
M : Meander No.
500
250
0
500 M

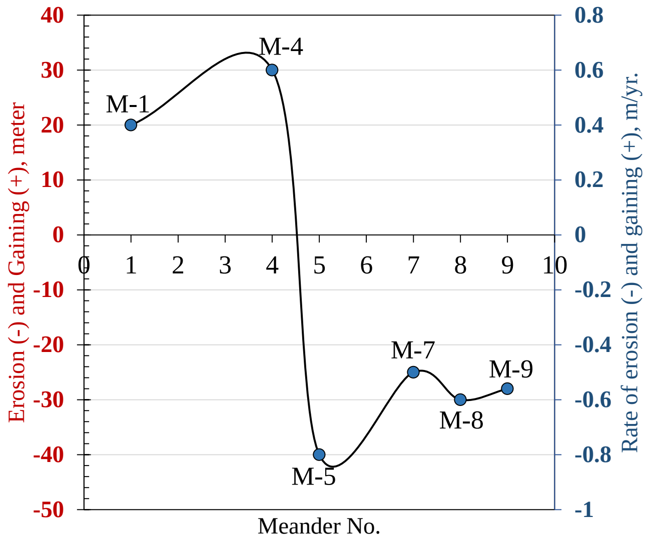
Erosion (-) and Gaining (+), meter
Rate of erosion (-) and gaining (+), m/yr.
Meander No.
40
30
20
10
0
-10
-20
-30
-40
-50
0.8
0.6
0.4
0.2
0
-0.2
-0.4
-0.6
-0.8
-1
0
1
2
3
4
5
6
7
8
9
10
M-1
M-4
M-5
M-7
M-8
M-9

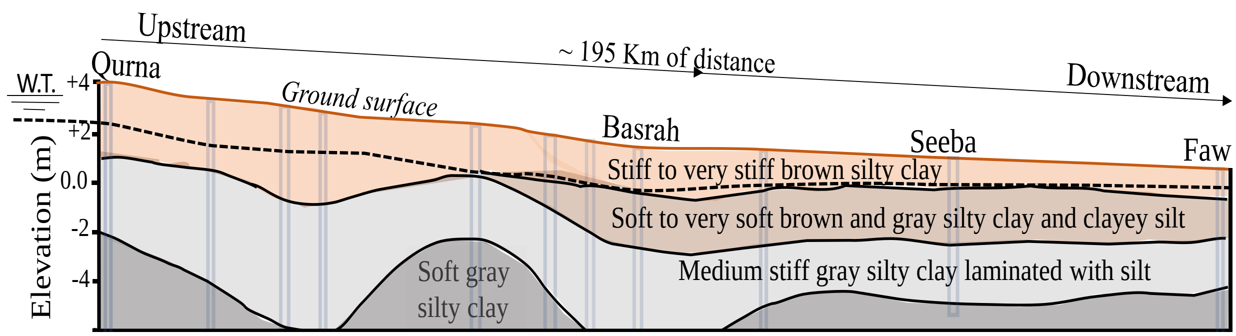

Upstream
~ 195 Km of distance
Downstream
Qurna
W.T.
Ground surface
Basrah
Seeba
Faw
Stiff to very stiff brown silty clay
Soft to very soft brown and gray silty clay and clayey silt
Medium stiff gray silty clay laminated with silt
Soft gray silty clay
Elevation (m)
+4
+2
0.0
-2
-4

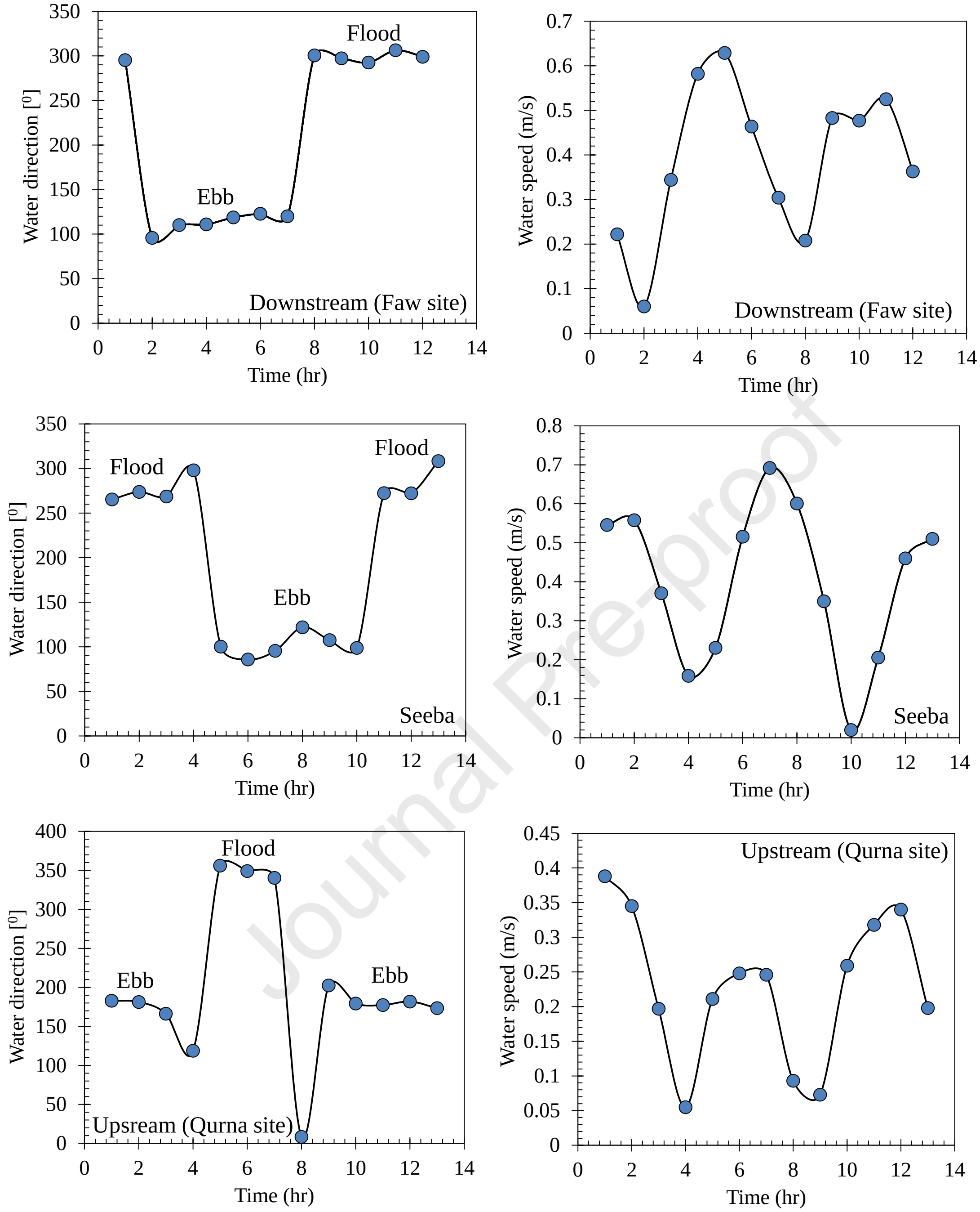
Water direction [°]
Flood
Ebb
Downstream (Faw site)
Time (hr)
Water speed (m/s)
Downstream (Faw site)
Time (hr)
Water direction [°]
Flood
Flood
Ebb
Seeba
Time (hr)
Water speed (m/s)
Seeba
Time (hr)
Water direction [°]
Flood
Ebb
Ebb
Upsream (Qurna site)
Time (hr)
Water speed (m/s)
Upstream (Qurna site)
Time (hr)

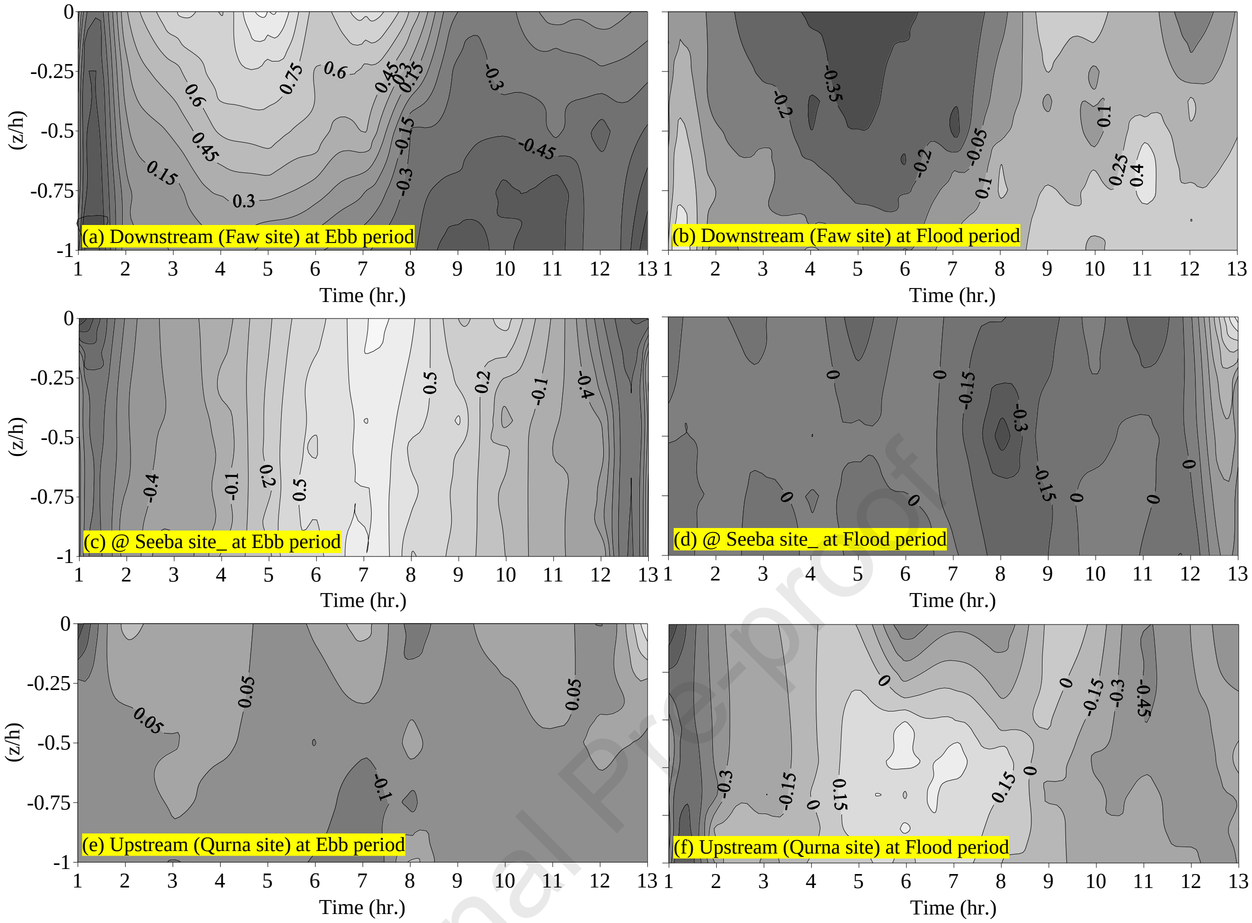
(a) Downstream (Faw site) at Ebb period
(b) Downstream (Faw site) at Flood period
(c) @ Seeba site_ at Ebb period
(d) @ Seeba site_ at Flood period
(e) Upstream (Qurna site) at Ebb period
(f) Upstream (Qurna site) at Flood period
(z/h)
Time (hr.)

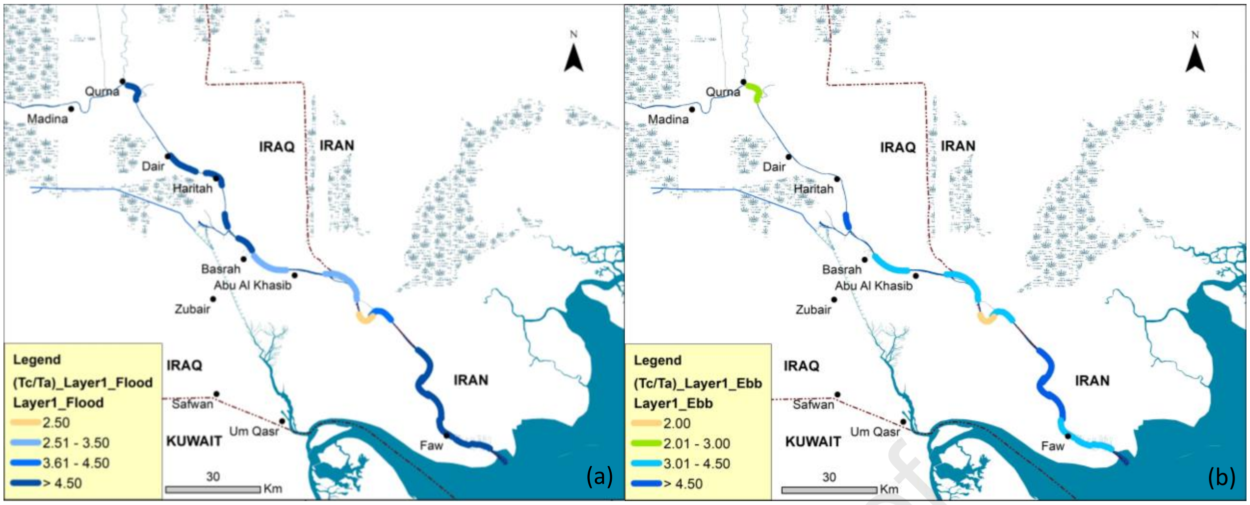
Qurna
Madina
Dair
Haritah
IRAQ
IRAN
Basrah
Abu Al Khasib
Zubair
IRAQ
Safwan
Um Qasr
KUWAIT
Faw
IRAN
Legend
(Tc/Ta)_Layer1_Flood
Layer1_Flood
2.50
2.51 - 3.50
3.61 - 4.50
> 4.50
30 Km
(a)
Legend
(Tc/Ta)_Layer1_Ebb
Layer1_Ebb
2.00
2.01 - 3.00
3.01 - 4.50
> 4.50
(b)

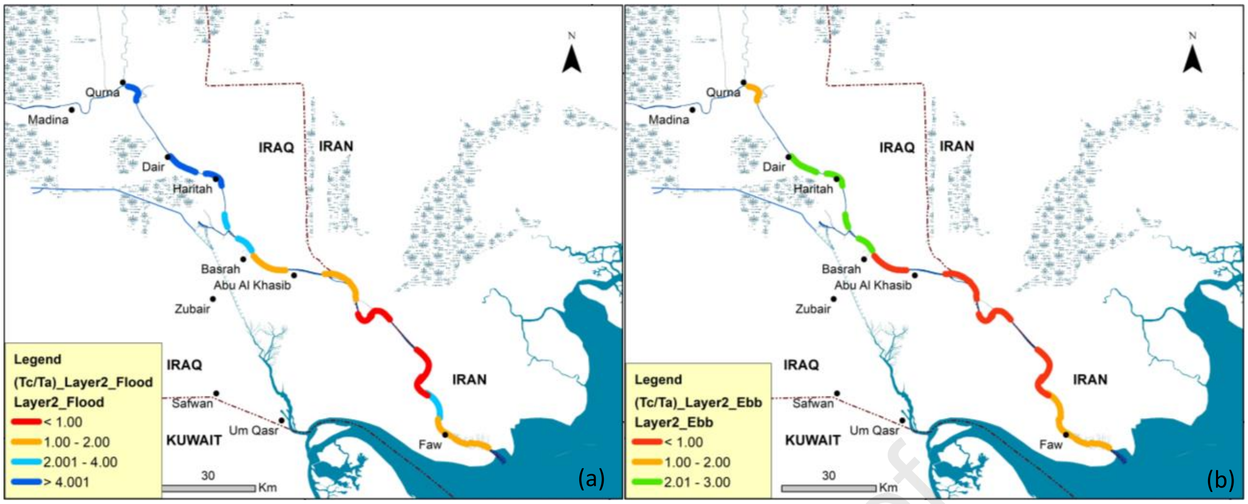
Qurna
Madina
Dair
Haritah
IRAQ
IRAN
Basrah
Abu Al Khasib
Zubair
IRAQ
Safwan
Um Qasr
KUWAIT
Faw
IRAN
Legend
(Tc/Ta)_Layer2_Flood
Layer2_Flood
< 1.00
1.00 - 2.00
2.001 - 4.00
> 4.001
30 Km
(a)
Qurna
Madina
Dair
Haritah
IRAQ
IRAN
Basrah
Abu Al Khasib
Zubair
IRAQ
Safwan
Um Qasr
KUWAIT
Faw
IRAN
Legend
(Tc/Ta)_Layer2_Ebb
Layer2_Ebb
< 1.00
1.00 - 2.00
2.01 - 3.00
30 Km
(b)

Highlights:

- Comprehensive evaluation of riverbank erosion along the tidal Shatt al Arab River in southern Iraq.
- variability in water velocities during flood and ebb phases creating distinct shear stresses affecting riverbanks.
- The ratio of critical (soil) shear stress to the fluid shear stress is a plausible way to understand better the susceptibility of the tidal riverbank retreat.
- hazardous erosion levels in southern and central river suggesting instability, while northern part exhibit relative stability.

Funding

The authors declare that no funding was received during the preparation of this research.

Declaration of competing interest

The authors declare that they have no known competing personal relationships or financial interests could have appeared to influence the work reported in this manuscript.